Structure and Dynamics of Maleic Anhydride

Stewart F. Parker,* Chick C. Wilson, John Tomkinson, David A. Keen, and Kenneth Shankland

ISIS Facility, Rutherford Appleton Laboratory, Chilton, Didcot, Oxon OX11 0QX, U.K.

Anibal J. Ramirez-Cuesta and Philip C. H. Mitchell

Department of Chemistry, University of Reading, Reading RG6 6AD, U.K.

Alastair J. Florence and Norman Shankland

Department of Pharmaceutical Sciences, University of Strathclyde, Glasgow G4 0NR U.K.

Received: October 16, 2000; In Final Form: January 4, 2001

We have carried out a comprehensive characterization of the structure and dynamics of maleic anhydride using experimental (single-crystal neutron diffraction, infrared, Raman and inelastic neutron scattering (INS) spectroscopies) and computational methods (AM1 and two levels of density functional theory). The structure is largely in agreement with previous work, although with more accurate atomic positions. However, the report of an unusually short C═C bond length is not supported by this work. The combination of ab initio results and INS spectra has confirmed the assignments of the internal modes. In addition, the complete lattice mode region is observed and assigned for the first time. Force fields derived by empirical means and from the ab initio data have been obtained and show differences, although both accurately predict the INS spectrum.

I. Introduction

Maleic anhydride is a widely used reagent in organic chemistry.[1] It is the simplest cyclic anhydride with a five-membered ring and provides a useful model compound for more complex systems such as the anhydrides used for the production of the resin component of advanced resin−fiber composites.[2] Maleic anhydride is also extensively used as a "functionalizing" agent in polyolefins.[3]

The structure has been determined by electron diffraction[4] and microwave spectroscopy[5,6] in the gas phase and by single-crystal X-ray diffraction in the solid state.[7] However, by contemporary standards, the structure is of low precision and, in particular, the hydrogen atom positions are not well-defined. This makes conclusions about the presence of possible C−H···O hydrogen bonds unreliable.

Maleic anhydride has been studied by vibrational spectroscopy in all three phases by a number of authors,[8−14] and empirical force fields[8,11,15,16] have been proposed. However, some of the out-of-plane modes are weak in both the infrared and Raman spectra and difficult to locate unambiguously. In addition there are disagreements in the assignments between the authors.

To resolve these problems, we have reinvestigated both the structure and dynamics of maleic anhydride. The structure has been determined by single-crystal neutron diffraction. The dynamics have been studied by infrared, Raman, and inelastic neutron scattering (INS) spectroscopies. The structure and assignments are supported by computational studies at three levels.

II. Experimental Section

Single-Crystal Neutron Diffraction. A single crystal of maleic anhydride of approximate dimensions $3 \times 2 \times 1.5$ mm^3 was obtained by slow evaporation of a saturated solution in ethyl acetate at room temperature. This was mounted inside a Displex refrigerator on a two-circle (χ,φ) orienter on the SXD time-of-flight Laue diffractometer at the ISIS spallation neutron source.[17,18] The data were collected at room temperature, with the diffraction measured by two arrays of position-sensitive detectors located at different scattering angles around the sample position. A series of 30 frames at different (χ,φ) settings were accumulated as described elsewhere,[17,18] with typical frame exposure times of 80−120 min. There was clear evidence of deterioration of the crystal during the course of the experiment (probably due to sublimation); scale factor refinements indicated an approximately 5-fold reduction in scattered intensity by the end of the experiment. Fortunately, the nature of the data collection, with many reflections collected simultaneously, allowed this to be normalized successfully. Unfortunately, the substantial crystal decay led to a limitation in the resolution.

The data were processed using standard SXD procedures. This resulted in a reasonable quality merged data set used for subsequent structural refinement.

Refinement was carried out on F^2, initially using GSAS,[19] and completed using SHELX-97.[20] The published X-ray structure[7] was used as the starting model. All atoms were refined with anisotropic atomic displacement parameters, including the hydrogen atoms. The details of the data collection parameters and refinements are summarized in Table S1 of the Supporting Information and the refined coordinates and thermal parameters in Table S2. Maleic anhydride: orthorhombic, space group $P2_12_12_1 \equiv D_2^4$ (No. 19), $Z = 4$, $a = 7.201(2)$ Å, $b = 11.342(7)$ Å, $c = 5.403(2)$ Å.

Vibrational Spectroscopy. Raman spectra were recorded using a Fourier transform Raman spectrometer (Perkin-Elmer 1760) with an InGaAs detector and ∼300 mW power at the sample using 1064 nm excitation from a Nd:YAG laser (Spectron). The samples were held in a brass sample holder in

* To whom all correspondence should be addressed. Fax: +44 1235 445120. E-mail: S.F.Parker@RL.AC.UK.

10.1021/jp0038005 CCC: $20.00 © 2001 American Chemical Society
Published on Web 03/06/2001

180° backscattering geometry. The spectra were recorded at 2 cm^{-1} resolution using the detector at room temperature (cutoff at ~3400 cm^{-1}, 40 scans) and at low temperature (cutoff at ~3000 cm^{-1}, 100 scans). In each case, the low-frequency limit of ~150 cm^{-1} was imposed by the filters used to reject the Rayleigh scattered 1064 nm radiation. The instrument has been described in detail elsewhere.[21]

Mid-infrared, 400−4000 cm^{-1}, spectra were recorded from KBr disks with a Digilab FTS-60 Fourier transform infrared (FTIR) spectrometer using 256 scans at 4 cm^{-1} resolution using triangular apodization with a room temperature deuterated triglycine sulfate (DTGS) detector. No further data processing was carried out.

The inelastic neutron scattering experiments were performed using the high-resolution broadband spectrometer (TFXA) at the ISIS pulsed spallation neutron source at the Rutherford Appleton Laboratory, Chilton, U.K. Full details of the spectrometer have been reported previously.[22] This is an inverted geometry time-of-flight spectrometer where a pulsed, polychromatic beam of neutrons illuminates the sample at 12 m from the source. The backscattered neutrons are Bragg reflected by a pyrolytic graphite analyzer, and those with a final energy of ~32 cm^{-1} are passed to the He^3 detector bank. Energy transfer and spectral intensity are then calculated using standard programs to convert to the conventional scattering law $S(Q,\omega)$. A consequence of the small final energy is that there is a unique value of momentum transfer Q ($Å^{-1}$) associated with each frequency ω (cm^{-1}). The trajectory is given by

$$Q^2 = \frac{1}{(2.0717)(8.0667)}(E_i + E_f - 2\sqrt{E_i}\sqrt{E_f}\cos\theta) \quad (1)$$

$$= 0.0598(E_i + 31.86 + 7.6990\sqrt{E_i})$$

where E_i and E_f (=31.86 cm^{-1}) are the incident and final energies, θ (=133°) is the scattering angle, and the constants are for the conversion of energy to wavevector.

TFXA offers high-resolution, ~2% $\Delta E/E$ between 16 and 4000 cm^{-1}. The sample was held in an aluminum sachet, cooled to ~20 K, and the spectrum was recorded for 12 h. The INS spectrum is available from the INS database[23] at the following Web address: www.isis.rl.ac.uk/insdatabase.

Computational Studies. Geometry optimization and normal mode calculations were carried out using both semiempirical (MNDO94 using the AM1 force field implemented as part of the CERIUS package) and ab initio methods. The latter used density functional theory (DFT) as implemented in GAUSSIAN98.[24] Two levels of theory were used, BP86 with the 6-21G basis set and B3LYP with the 6-31G(d,p) basis set. The GAUSSIAN98 output includes the atomic displacements in each mode; these were used to generate the INS spectrum using the program CLIMAX.[25] Included in CLIMAX is the method of Allouche and Pourcin[26] which transforms the Cartesian force constants calculated by GAUSSIAN98 into internal coordinate force constants as described previously.[27] This allows refinement of the force constants in either internal or symmetry coordinates as desired.

Materials. Maleic anhydride (99%) was obtained from Aldrich and used without further purification.

III. Results

Structure. The refined atomic parameters are given in Table S2 of the Supporting Information, with bond lengths and angles in Table 1. Two views of the structure are shown in Figure 1. Clearly we have obtained a good quality refinement even from the decaying crystal. We subjected the thermal parameters to further analysis to verify the earlier conclusions from the X-ray study. This analysis was carried out in the program THMA11[28] and reasonable fits were obtained. The molecular vibrations are fairly well described by the rigid body model apart from the hydrogen atoms and to a lesser extent the carbonyl oxygen atoms which exhibit slightly enhanced thermal motions. These are difficult to quantify precisely from our data and are perhaps best illustrated by the ORTEP[29] plot in Figure 1, from which it can be seen that the slightly enhanced motions of the oxygen atoms are out of the plane of the molecule, but these effects are rather small.

TABLE 1: Comparison of Structural Parameters

bond	neutron	X-ray[7]	microwave[5]	MNDO	BP86	B3LYP
			bond lengths (Å)			
O1−C2	1.399(9)	1.393(5)	1.3876(1)	1.409	1.456	1.393
O1−C5	1.369(9)	1.383(5)	1.3876(1)	1.409	1.456	1.393
C2−C3	1.463(8)	1.467(5)	1.4849(3)	1.497	1.505	1.491
C5−C4	1.480(8)	1.472(5)	1.4849(3)	1.497	1.505	1.491
C2═O6	1.202(11)	1.184(5)	1.1962(1)	1.216	1.227	1.198
C5═O7	1.209(11)	1.194(5)	1.1962(1)	1.216	1.227	1.198
C3═C4	1.328(9)	1.303(5)	1.3331(1)	1.349	1.348	1.336
C3−H8	1.094(16)	1.11(15)	1.0791(3)	1.091	1.087	1.082
C4−H9	1.077(15)	1.05(15)	1.0791(3)	1.091	1.087	1.082
			bond angles (deg)			
C5−O1−C2	107.7(5)	107.5(1.0)	108.06(1)	107.5	107.1	108.6
O1−C2−C3	108.1(5)	107.8(1.0)	108.07(1)	108.3	107.1	107.5
O1−C5−C4	108.3(6)	107.6(1.0)	108.07(1)	108.3	107.1	107.5
O1−C2═O6	122.0(7)	121.3(1.0)	122.32(1)	117.0	122.2	122.7
O1−C5═O7	120.5(7)	120.1(1.0)	122.32(1)	117.0	122.2	122.7
C3−C2═O6	129.9(8)	130.9(1.0)	129.61(1)	134.7	130.6	129.7
C4−C5═O7	131.2(7)	132.3(1.0)	129.61(1)	134.7	130.6	129.7
C2−C3═C4	108.1(5)	108.3(1.0)	107.90(1)	108.0	109.3	108.1
C3═C4−C5	107.8(5)	108.8(1.0)	107.90(1)	108.0	109.3	108.1
C2−C3−H8	123.1(11)	120(10.0)	122.10(1)	121.6	121.9	122.1
C5−C4−H9	120.6(12)	125(10.0)	122.10(1)	121.6	121.8	122.1
C4═C3−H8	128.8(11)	131(10.0)	129.99(1)	130.4	128.8	129.8
C3═C4−H9	131.6(12)	126(10.0)	129.99(1)	130.4	128.8	129.8

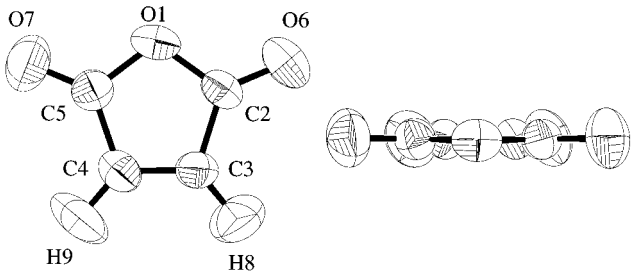

Figure 1. ORTEP[29] plots of the maleic anhydride structure at 295 K showing the atomic numbering. Probability ellipsoids drawn at the 50% level. The slightly enhanced thermal motions of the carbonyl oxygens and the hydrogen atoms can be seen, and there is an indication this enhancement is out of the plane of the molecule.

The pattern of nonbonded contacts found also confirms the findings of the previous X-ray study, though with the far superior determination of the hydrogen atoms in our current neutron diffraction study, these are now fully quantified. The closest nonbonded contacts involve the hydrogen atoms and the carbonyl oxygen atoms of neighboring molecules, as indicated in Table 2.

However, these contacts are all very long, and as found in the X-ray study, the geometry of these (C−H···O angles) is not indicative of hydrogen-bonded interactions. We confirm here the existence of a loosely linked network of maleic anhydride molecules vibrating in a manner fairly well described by rigid body motion, with the atoms extrinsic to the ring undergoing

TABLE 2: Non-Bonded Intermolecular Close Contacts in Maleic Anhydride (Distances in Angstroms, Angles in Degrees)

C−H	H···O	∠(CHO)	nonbonded contact
1.094(16)	2.652(20)	157(1)	C3−H8···O6 at $[x - {}^1/_2, {}^1/_2 - y, -z - 2]$
1.094(16)	2.606(21)	103(1)	C3−H8···O7 at $[-x, {}^1/_2 + y, -{}^3/_2 - z]$
1.077(15)	2.803(19)	139(1)	C4−H9···O6 at $[-x, y - {}^1/_2, -z - {}^3/_2]$
1.077(15)	2.929(19)	125(1)	C4−H9···O7 at $[-x - {}^1/_2, -y, z - {}^1/_2]$

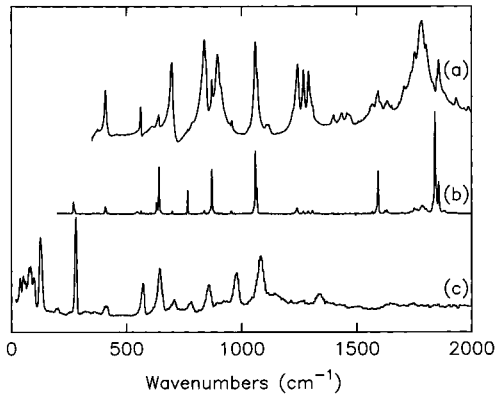

Figure 2. Vibrational spectra of maleic anhydride: (a) infrared (at room temperature), (b) Raman (at room temperature), and (c) inelastic neutron scattering spectrum (at 20 K).

slightly enhanced and directional additional vibrational motions. The weak nature of the interactions undergone by these terminal atoms suggest that these are not the controlling factor in determining the magnitude of additional thermal motion.

Vibrational Spectroscopy. The idealized structure of maleic anhydride is C_{2v}, and the electron diffraction[4] results in the gas phase as well as the infrared and Raman spectra in the gas phase and in solution are consistent with this structure.[8−14] Confirmation has come from gas-phase microwave[5,6] spectroscopy that employed extensive isotopic substitution to show that the structure was unambiguously C_{2v}. As shown in the previous section, in the solid state at room temperature, the molecule occupies a C_1 site, but, as can be seen from Table 1, the molecular symmetry is very close to C_{2v}. For an isolated C_{2v} molecule the internal modes are classified as $8A_1 + 7B_1 + 3A_2 + 3B_2$ (with A_1 and B_1 the in-plane modes). There are four molecules in the unit cell; thus, each vibration gives rise to four modes in the unit cell (factor group splitting). The similarity of the infrared and Raman frequencies demonstrates that for most of the internal modes the factor group splitting is negligible.

Figure 2 shows the infrared, Raman, and INS spectra of maleic anhydride. Similarities and differences are apparent between all three spectra and emphasize the need to have all three types of spectra for a complete analysis. The three forms of vibrational spectroscopy exploit different properties of the molecule. Infrared spectroscopy requires a change in dipole moment and thus is sensitive to the polar motions of the molecule, while Raman spectroscopy requires a change in polarizability and thus is more sensitive to the nonpolar motions of the molecule. These two techniques provide information on the heavy atom motions of the molecule, e.g., $\nu_{C=C}$, $\nu_{C=O}$. In contrast, the INS spectrum is dominated by the hydrogenic motions. This arises because the intensity of an INS band is proportional to the product of the inelastic scattering cross-section and the amplitude of vibration. Since the scattering cross-section for hydrogen is at least 20 times larger than for any other type of atom present in the molecule, the INS spectrum emphasizes the modes that involve substantial hydrogen motion either directly (e.g., C−H bend) or where the hydrogen is "riding" on another atom (e.g., torsions or other ring deformations).

TABLE 3: Frequencies (cm^{-1}) and Assignments of the Fundamental Bands of Maleic Anhydride[a]

IR	Raman	INS	assignment
3132m	3132		C−H stretch (ν_1, A_1)
3124m	3124		C−H stretch (ν_9, B_1)
1857m	1841vs		C═O stretch (ν_2, A_1)
1787s	1763w	1747w	C═O stretch (ν_{10}, B_1)
1593m	1593s		C═C stretch (ν_3, A_1)
	1307w	1338m	C−H ip bend (ν_{11}, B_1)
		1261w	
1059s	1059s	1084s	C−H ip bend (ν_5, A_1)
958vw		978s	C−H oop bend (ν_{16}, A_2)
871w	871s	859s	C−H oop bend (ν_{19}, B_2)
	767m	781w	ring def (ν_{17}, A_2)
698s	707w	707w	ring def (ν_{14}, B_1)
641w	642s	645s	ring def (ν_{20}, B_2)
562m	564vw	572s	C═O ip bend (ν_{15}, B_1)
409m	408w	412w,br	C═O ip bend (ν_8, A_1)
	270m	280vs	C═O oop bend (ν_{18}, A_2)
		199w,br	C═O oop bend (ν_{21}, B_2)
120s	115sh	127vs,br	*a*-axis libration
100w	95sh	98s	*c*-axis libration
		85s	*b*-axis libration
		78s	*b*-axis libration
	65vs	60s	translational
	52vs	54s	and
	43sh	41sh	acoustic
	28vs	39s	modes

[a] s = strong, m = medium, w = weak, br = broad, v = very, ip = in-plane, oop = out-of-plane.

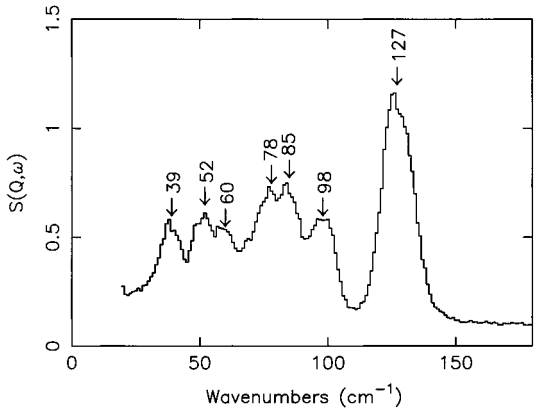

Figure 3. External mode region of the INS spectrum of maleic anhydride at 20 K.

The INS spectrum shows unambiguously some of the modes that have been difficult to observe previously. In particular, the B_1 C−H in-plane bend at 1337 cm^{-1} that only appears as a shoulder in the infrared spectrum and as a very weak band in the Raman spectrum is clearly seen in the INS spectrum. Most of the medium and strong bands below 1000 cm^{-1} in the INS spectrum are the out-of-plane modes and provide confirmation of earlier assignments. Table 3 lists the observed bands and their assignments. For the internal modes, the assignments are in agreement with those of Rogstad et al.[11]

The external mode region is shown in Figure 3 and has not been previously assigned. For an isolated C_{2v} molecule the librations are of B_1, B_2, and A_2 character. From the neutron structure and with the usual convention that the moments of inertia obey $I_c \geq I_b \geq I_a$ we calculate that $I_c = 4.58 \times 10^{-45}$, $I_b = 3.36 \times 10^{-45}$, and $I_a = 1.23 \times 10^{-45}$ kg m^2; thus the axes

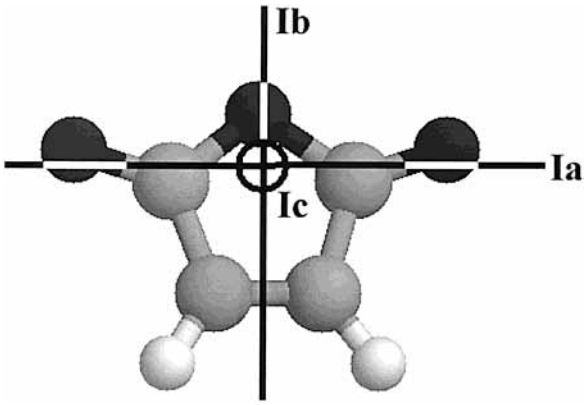

Figure 4. Positions of the inertial axes in maleic anhydride.

are as shown in Figure 4. By inspection, the A_2 libration is associated with I_c, B_1 with I_b, and B_2 with I_a. Since I_a is much smaller than I_c and I_b, the highest external mode at 127 cm^{-1} is assigned to the B_2 libration associated with I_a. In the far-infrared spectrum[10] a very strong band at 110 cm^{-1} that shifts to 120 cm^{-1} at 77 K is observed; since the B_2 modes give strong infrared bands, this is consistent with our assignment for this mode.

In an isotropic field, the librations would be proportional to the inverse square root of the moments of inertia, so the other two librations are predicted at 77 and 66 cm^{-1}. Hence, the bands centered at 98 and 80 cm^{-1} are assigned to the B_1 (I_b) and A_2 (I_c) modes; the deviations are assumed to be due to the structure being orthorhombic rather than cubic.

The observed INS intensities can be used to support these assignments. The intensity of an INS band at ω_i is given by[22]

$$S(Q,\omega_i) \propto Q^2 U_i^2 \exp(-Q^2(U_{Ext}{}^2 + U_{Int}{}^2)) \qquad (2)$$

where U_i is the amplitude of vibration of the mode at ω_i, the exponential term is the Debye−Waller factor with $U_{Ext}{}^2$ and $U_{Int}{}^2$ the total mean square displacement of the external and internal modes, respectively. For the librational modes $U_{Ext}{}^2$ is the same for all the modes. Since the hydrogen cross-section is much larger than for any other atom, the contribution from the motion of the hydrogen atoms will dominate this term. The crystallography has shown that the angular displacement about all three inertial axes is the same; thus, the amplitude of motion will be directly proportional to the perpendicular distance of the hydrogen atoms from the axis of libration. The average distances are 2.11, 1.36, and 2.52 Å for I_a, I_b, and I_c, respectively. From eq 1 the Q value for each mode is obtained; hence, the ratio of the intensities using the assignments given above is predicted to be as follows: $I_a/I_b = 2.98$, $I_a/I_c = 1.03$, and $I_b/I_c = 0.34$. These are in good agreement with the measured ratios $I_{127}/I_{98} = 2.67$, $I_{127}/I_{80} = 1.24$, and $I_{98}/I_{80} = 0.46$ and lend strong support to the assignments.

The two lowest energy features centered at 41 and 56 cm^{-1} are assigned to the translations. The four molecules give rise to 12 modes, three acoustic and nine optic. The temptation is to assign the 41 cm^{-1} feature to the acoustic modes and the 56 cm^{-1} to the optic modes. This is untenable for two reasons. If it was correct, then the ratio of the INS intensities of the bands should be ∼1:3 (acoustic:optic). Including the correction for the different Q values, the measured ratio is 1:1.21, clearly incompatible with the assignment. In addition, the low-frequency Raman spectrum[13] shows strong bands at 28 and 52 cm^{-1}. Since acoustic modes have zero frequency at zero wavevector, they are not normally observable by optical spectroscopy. It follows that the 28 and 52 cm^{-1} bands in the Raman spectrum must be optic modes and that both groups of bands seen in the INS spectrum contain contributions from both the acoustic and optic modes. Table 3 gives a list of the fundamental frequencies and their assignments.

Computational Studies. The structural parameters calculated by the three levels of theory are given in Table 2. All three methods were run with no imposed symmetry; all three found a minimum with planar geometry and C_s symmetry. Inspection of Table 1 shows that to four significant figures the symmetry is in fact C_{2v}. All three methods are an isolated molecule approach; thus, the gas-phase geometry is the reference point. As would be expected, comparison with the gas-phase structure (as determined by microwave spectroscopy[5,6]) shows that the agreement improves with increasing level of theory. The rotational constants and dipole moment as determined by microwave spectroscopy[5,6] show similarly good agreement: (B3LYP results in brackets): $I_c = 4.6270\ (4.6572) \times 10^{-45}$, $I_b = 3.4007\ (3.4303) \times 10^{-45}$, and $I_a = 1.2264\ (1.2269) \times 10^{-45}$ kg m^2, 4.14 (4.31) D.

A similar pattern is evident with the vibrational frequencies; see Table 4. Comparison with the (incomplete) gas-phase frequencies gives a root mean square deviation (omitting the C−H stretch mode, since anharmonicity is likely to be significant here) of 60.9, 20.5, and 12.4 cm^{-1} for the AM1, BP86, and B3LYP models, respectively. If the C═O stretch frequencies are also omitted, the results are: 30.5, 15.3, and 7.7 cm^{-1}.

From the assignments given in Table 3 an empirical force field was developed using CLIMAX.[24] This used the in-plane force constants of Mirone and Chiorboli[8] as initial parameters and assumed C_{2v} symmetry. For comparison the force field in internal coordinates was generated in CLIMAX from the Cartesian force field output by Gaussian.[25,26] The INS spectra calculated from each force field are shown in Figure 5. The final values for the complete force fields are given in Table 5.

The potential energy distribution, Table S6 of the Supporting Information, shows that the traditional descriptions of the modes are basically correct, although most of the modes have large contributions from other types of motion. The two lowest energy modes, which are usually described as C═O out-of-plane bending are better described as in- and out-of-phase C−O torsions, with the carbonyl out-of-plane modes at higher energy.

IV. Discussion

The structure determined by single-crystal neutron diffraction is in good agreement with the previous X-ray determination[7] but with much greater accuracy with regard to the hydrogen atom positions. The major difference is that the apparently anomalously short C═C distance of 1.303(5) Å is not substantiated; instead a much more normal C═C distance of 1.328(9) Å is obtained. While the precision of our study is somewhat limited by the crystal decay, the C═C bond length we find appears to be significantly longer than in the X-ray study and is closer to the C═C distance found in maleic acid[30] (1.337 Å) and disodium maleate monohydrate[31] (1.336 Å) by single-crystal X-ray diffraction. (For comparison, the gas-phase ethylene C═C distance[32] is 1.3338 Å.)

The structural analysis also suggested that the thermal ellipsoids for the carbonyl oxygen atoms and the hydrogen atoms were enhanced out of the plane of the molecule. The two lowest modes involve carbonyl motion out of the molecular plane, and the frequencies correspond to temperatures of 290 and 403 K.

TABLE 4: Comparison of Observed and Calculated Frequencies (cm^{-1})

		experimental[a]		calculated		
mode		gas	solid	MNDO	BP86	B3LYP
A_1						
ν_1	C−H sym stretch		3132	3252	3213	3278
ν_2	C═O sym stretch	1865	1857	2195	1774	1928
ν_3	C═C stretch		1595	1771	1588	1664
ν_4	C−O sym stretch	1232	1243	1300	1155	1276
ν_5	C−H ip bend		1066	1098	1041	1081
ν_6	C−C sym stretch		872	1086	771	876
ν_7	ring def		641	761	597	637
ν_8	C═O ip bend		415	383	364	400
B_1						
ν_9	C−H asym stretch	3120	3124	3239	3189	3257
ν_{10}	C═O asym stretch	1805	1785	2113	1704	1866
ν_{11}	C−H ip bend		1309	1384	1295	1337
ν_{12}	C−O asym stretch	1055	1059	1200	960	1062
ν_{13}	C−C asym stretch		896	1052	793	911
ν_{14}	ring def	699	697	696	650	703
ν_{15}	C═O ip bend	556	563	522	517	559
A_2						
ν_{16}	C−H oop bend		959	978	964	978
ν_{17}	ring def		768	704	718	762
ν_{18}	C═O oop bend		275	267	267	264
B_2						
ν_{19}	C−H oop bend	840	839	914	833	853
ν_{20}	ring def		631	602	606	640
ν_{21}	C═O oop bend	161	200	156	161	168

[a] Gas-phase frequencies are from ref 11. The solid-state frequencies below 1500 cm^{-1} are from the INS spectrum; those above 1500 cm^{-1} are from ref 9.

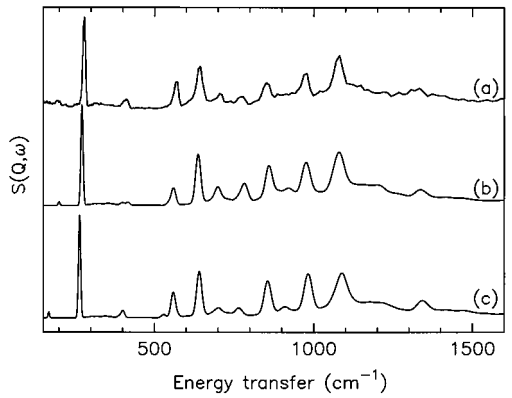

Figure 5. Comparison of the experimental (a) and calculated INS spectrum of maleic anhydride using the empirically (b) and ab initio (c) derived force fields.

Thus, a substantial population of the modes at room temperature is expected, accounting for the distortion in the thermal ellipsoids.

The crystallography has shown that C−H···O hydrogen-bonding is absent. The question thus remains, "what holds the structure together?" For comparison, heptane with almost the same molecular weight melts at −91 °C and boils at 98 °C, whereas maleic anhydride melts at 55 °C and boils at 200 °C. A matrix isolation study[12] found that the gas-to-matrix shifts were small (all $<\pm 20$ cm^{-1}, most $<\pm 10$ cm^{-1}) and very similar to the gas-to-solid shifts. Microwave spectroscopy[6] has shown that maleic anhydride has a substantial dipole moment of 4.14 D; thus, a reasonable suggestion is that it is the dipole−dipole interaction that is responsible for the anomalous physical properties.

The largest discrepancy between the experimental and ab initio frequencies is for the C═O modes, both of which are calculated about 60 cm^{-1} (3.4%) too high. This is not uncommon with DFT calculations; recent work on thymine[33] and oxamide[34] showed similar errors. This is not a failing of the isolated molecule approximation; for thymine the comparison was with the matrix isolated molecule and for oxamide a pentamer was considered. For thymine, the difference was ascribed to anharmonicity of the carbonyl stretch. In the present case, the combination band from ($C{=}O_{sym}$ + $C{=}O_{asym}$) is at the same frequency as the sum of the individual frequencies, indicating that the anharmonicity is small.

A comparison of the empirical and ab initio force fields reveals some interesting points. An empirical force field is usually developed on the basis of some guiding principles. In particular, the aim is to minimize the number of force constants, particularly the off-diagonal interaction constants. This is because the number of elements in the force constant matrix is normally much greater than the number of observed frequencies, hence the need for extensive isotopic substitution. The use of INS data ameliorates the problem because the intensities as well as the frequencies can be used. For modes below ~1600 cm^{-1} this basically doubles the number of experimental observations. To reduce the number of parameters, it is customary to assume that modes that are separated in frequency by more than about 500 cm^{-1} do not interact; thus, C−H stretching frequencies are often treated in isolation. There is also an expectation that interaction constants will fall in the range ± 0.5 mdyn/Å; those that fall outside this range are usually regarded with suspicion.

The empirical force field developed here has been generated with these ideas in mind and conforms to them. This is to be contrasted with the ab initio force field. The *only* terms that are zero are those that are enforced by symmetry, (in-plane and out-of-plane coordinates do not mix because there are no symmetry elements that couple them). As shown in Table 5, the diagonal terms from the DFT tend to be smaller than with the empirical force field, while the off-diagonal terms are often much larger and values greater than 1.0 occur. In essence, it appears that the ab initio calculation is more "democratic" with less distinction between the diagonal and off-diagonal terms than is customary with empirical force fields.

TABLE 5: Comparison of Force Constants

coordinate	Di Lauro	Giorgini	empirical	B3LYP
		Diagonal Constants		
stretches				
C1−O2	4.064		4.371	3.1930
C1−O5	4.064		4.371	3.1928
C2−C3	4.360		4.990	3.0362
C4−C5	4.360		4.990	3.0363
C3═C4	8.928		8.898	6.7057
C2═O6	10.298		9.300	14.3390
C5═O7	10.298		9.300	14.3374
C3−H9	5.324		5.324	5.8302
C4−H8	5.324		5.324	5.8300
in-plane bends				
C5−O1−C2	1.585		1.585	1.1254
O1−C2−C3	1.618		1.618	0.6962
O1−C5−C4	1.618		1.618	0.6962
C2−C3═C4	1.157		1.157	0.6974
C3═C4−C5	1.157		1.157	0.6974
O1−C2═O6	1.532		1.532	0.7308
O1−C5═O7	1.532		1.532	0.7307
C3−C2═O6	0.548		0.548	0.5935
C4−C5═O7	0.548		0.548	0.5935
C2−C3−H9	0.347		0.347	0.3941
C5−C4−H8	0.347		0.347	0.3941
C4═C3−H9	0.464		0.464	0.3878
C3═C4−H8	0.464		0.464	0.3878
out-of-plane bends				
C2═O6 oop		0.740	0.750	0.5052
C5═O7 oop		0.740	0.750	0.5050
C3−H9 oop		0.183	0.225	0.2313
C4−H8 oop		0.183	0.225	0.2313
torsions				
O1−C2 tor		0.128	0.179	0.1001
O1−C5 tor		0.128	0.179	0.1001
C2−C3 tor		0.225	0.247	0.1122
C4−C5 tor		0.226	0.247	0.1122
C3═C4 tor		0.315	0.291	0.2299
		Interaction Constants		
stretch/stretch				
C−O/ C−O	1.190		1.068	0.3675
C−O/C−C	1.115		1.231	−0.0358
C−O/C═O	0.750		0.708	1.0160
C−O/C═C				1.7554
stretch/bend				
C−O/O−C═O	0.285		0.407	0.4040
C−C/C−C═O	0.440		0.389	0.2483
C−C/C−C═C	0.155			−0.2320
C═C/C═C−H	0.278		0.203	0.5090
C═C/C═C−C				−0.8541
out-of-plane bend/out-of-plane bend				
C═O oop/ C═O oop			−0.130	0.0330
C-H oop/C−H oop		−0.015	−0.035	−0.0150
torsion/torsion				
C═C tor/C−C tor		−0.029		
C−C tor/C−C tor		−0.050		
torsion/out-of-plane bend				
C−O tor/C═O oop			−0.048	
C═C tor/C═O oop			−0.034	
C−O tor/C−H oop			0.021	

This raises the question, "which is correct?" As judged by the INS spectra that each force field generates, both are equally good; see Figure 5. The potential energy distribution from both force fields is similar, as shown in Table S6 of the Supporting Information. Thus, from a practical viewpoint there is little to choose between them. From the purist view, the ab initio force field is better because it produces a unique solution in as far as the ab initio calculation is correct (note that implicit in the ab initio is the assumption of the isolated molecule approximation and the harmonic approximation), whereas the empirical force field is convenient but is not unique. However, as indicated in the Introduction, one of the aims of the work is to apply the force fields to more complex systems; thus, transferability is important, and this is clearly easier with the smaller empirical force field.

Acknowledgment. The Rutherford Appleton Laboratory is thanked for access to neutron beam facilities.

Supporting Information Available: Table S1 giving details of the single-crystal neutron diffraction data collection and refinement, Table S2 listing the crystallographic data (a, fractional atomic coordinates and equivalent isotropic thermal parameters; b, the anisotropic displacement parameters) for

maleic anhydride at 295 K from the neutron diffraction experiment, Table S3 giving the bond lengths and angles for maleic anhydride at 295 K from the neutron experiment, Table S4 detailing the definition of internal coordinates of maleic anhydride, Table S5 listing the ab initio force constants from B3LYP in the internal coordinates defined in Table S4, Table S6 comparing the potential energy distribution from the empirical and ab initio force fields. This material is available free of charge via the Internet at http://pubs.acs.org.

References and Notes

(1) Finar, I. L.*Organic Chemistry,* 6th ed., Vol. 1; Longman: Hong Kong, 1973; pp 536−539.

(2) Wilson, D., Stenzburger, H. D., Hergenrother, P. M., Eds. *Polyimides;* Blackie: Glasgow, 1990.

(3) De Roover, B.; Sclavons, M.; Carlier, V.; Devaux, J.; Legras, R.; Momtaz, A. *J. Polym. Sci. Part A: Polym. Chem.* **1995,** *33,* 829.

(4) Hilderbrandt, R. L.; Peixoto, J. *J. Mol. Struct.* **1972,** *12,* 31.

(5) Stiefvater, O. L. *Z. Naturforsch.* **1977,** *32A,* 1480.

(6) Alonso, J. L.; Pastrana, M. R.; Pelaez, J.; Arauzo. *Spectrochim. Acta* **1983,** *39A,* 215.

(7) Marsh, R. E.; Ubell, E.; Wilcox, H. E. *Acta Crystallogr*. **1962,** *15,* 35.

(8) Mirone, P.; Chiorboli, P. *Spectrochim. Acta* **1962,** *18,* 1425.

(9) di Lauro, C.; Califano, S.; Adembri, G. *J. Mol. Struct.* **1968,** *2,* 173.

(10) Baranska, H., Christensen, D. H.; Nicholaisen, F.; Nielsen, Klaboe, P.; O. F.; *Acta Chem. Scand.* **1971,** *25,* 2365.

(11) Rogstad, A.; Klaboe, P.; Baranska, H.; Bjarnov, E.; Christensen, D. H.; Nicholaisen, F.; Nielsen, O. F.; Cyvin; B. N.; Cyvin, S. J. *J. Mol. Struct.* **1974,** *20,* 403.

(12) Barnes, J.; Le Gall, L.;. Madec, C.; Lauransan, *J. Mol. Struct.* **1977,** *38,* 109.

(13) Ishibashi, Y.; Shimada, R.; Shimada, H. *Bull. Chem. Soc. Jpn.* **1982,** *55,* 2765.

(14) Jordanov, B.; Nentchovska, R.; Schrader, B. *J. Mol. Struct.* **1993,** *297,* 401.

(15) Le Gall, L.; Caillet, P.; Forel, M.-T. *J. Chim. Phys.* **1978,** *75,* 444.

(16) Giorgini, M. G. *J. Mol. Struct.* (*THEOCHEM)* **1983,** *94,* 37.

(17) Wilson, C. C. Data analysis of reciprocal space volumes. In *Neutron Scattering Data Analysis 1990*, Johnson, M. W., Ed.; IoP Conference Series Vol. 107; Adam Hilger: Bristol, U.K., 1990; pp 145−163.

(18) Wilson, C. C. *J. Mol. Struct.* **1997**, *405*, 207.

(19) Larsen, A. C.; von Dreele, R. B., *GSAS, General Structure Analysis System*; Report LAUR-86-748; Los Alamos National Laboratory: Los Alamos, NM, 1994.

(20) Sheldrick G. M. *SHELXL-97*, a program for crystal structure refinement; University of Göttingen: Göttingen, Germany, 1997.

(21) Crookell, A.; Hendra, P. J.; Mould, H. M.; Turner, A. J. *J. Raman Spectrosc*. **1990,** *21,* 85.

(22) Tomkinson, J. In *Recent Experimental and Computational Advances in Molecular Spectroscopy*; Fausto R., Ed.; Kluwer: Amsterdam, 1993; pp 229−249.

(23) Parker, S. F.; Champion, D. *Internet J. Vib. Spectrosc.* 1999, *3* [http://www.ijvs.com/volume3/edition3/section1.htm#Ed].

(24) Frisch, M. J.; Trucks, G. W.; Schlegel, H. B.; Scuseria, G. E.; Robb, M. A.; Cheeseman, J. R.; Zakrzewski, V. G.; Montgomery, Jr., J. A.; Stratmann, R. E.; Burant, J. C.; Dapprich, S.; Millam, J. M.; Daniels, A. D.; Kudin, K. N.; Strain, M. C.; Farkas, O.; Tomasi, J.; Barone, V.; Cossi, M.; Cammi, R.; Mennucci, B.; Pomelli, C.; Adamo, C.; Clifford, S.; Ochterski, J.; Petersson, G. A.; Ayala, P. Y.; Cui, Q. Morokuma, K.; Malick, D. K.; Rabuck, A. D.; Raghavachari, K.; Foresman, J. B.; Cioslowski, J.; Ortiz, J. V.; Stefanov, B. B.; Liu, G. Liashenko, A.; Piskorz, P.; Komaromi, I.; Gomperts, R.; Martin, R. L.; Fox, D. J.; Keith, T.; Al-Laham, M. A.; Peng, C. Y.; Nanayakkara, A.; Gonzalez, C.; Challacombe, M.; Gill, P. M.; W. Johnson, B.; Chen, W.; Wong, M. W.; Andres, J. L.; Gonzalez, C.; Head-Gordon, M.; Replogle, E. S.; Pople, J. A. *Gaussian 98*, Revision A.3; Gaussian, Inc.: Pittsburgh, PA, 1998.

(25) Kearley, G. J. *Nucl. Inst. Methods Phys. Res. A* **1995,** *354,* 53.

(26) Allouche, A.; Pourcin, J. *Spectrochim. Acta* **1993,** *49A,* 571.

(27) Kearley, G. J.; Tomkinson, J.; Navarro, A.; López-González, J. J.; Fernández-Gómez, M. *Chem. Phys.* **1997,** *216,* 323.

(28) Trueblood, K. N.; Huber-Buser, E. *THMA11, program for analysing thermal parameters*, University of California: Los Angeles, 1987.

(29) Johnson, C. K. *ORTEP, Thermal Ellipsoid Plotting Program*; Report ORNL-3794; Oak Ridge National Laboratory: Oak Ridge, TN, 1971. Program version used: ORTEP-III by C. K. Johnson and M. N. Burnett, implemented as ORTEP 3 for Windows (Farrugia, L. J. University of Glasgow).

(30) James, M. N. G.; Williams, G. J. B. *Acta Crystallogr*. **1974,** *B30,* 1249.

(31) James, M. N. G.; Williams, G. J. B. *Acta Crystallogr*. **1974,** *B30,* 1257.

(32) Duncan, J. L. *Mol. Phys.* **1974,** *28,* 1177.

(33) Szczepaniak, K.; Szczepaniak, M. M.; Person, W. B. *J. Chem. Phys. A* **2000,** *104,* 3852.

(34) Hudson, B. S.; Tse, J.; Zgierski, M. Z.; Parker, S. F.; Braden, D. A.; Middleton; C. *Chem. Phys.* **2000,** *261,* 249.